THE JOURNAL OF PHYSICAL CHEMISTRY A LETTERS

2009, *113,* 1674–1677
Published on Web 02/11/2009

Hot Brownian Particles and Photothermal Correlation Spectroscopy

Romy Radünz,*,† Daniel Rings,‡ Klaus Kroy,‡ and Frank Cichos†

Molecular Nanophotonics, Institute of Experimental Physics I, University of Leipzig, Linnestrasse 5, 04103 Leipzig, Germany, and Soft Condensed Matter Theory, Institute of Theoretical Physics, University of Leipzig, Vor dem Hospitaltore 1, 04103 Leipzig, Germany

Received: November 28, 2008; Revised Manuscript Received: January 30, 2009

We introduce a new technique to measure tracer dynamics, which is sensitive to single metal nanoparticles down to a radius of 2.5 nm with a time resolution of a few microseconds. It is based on a fluctuation analysis of a heterodyne photothermal scattering signal emanating from the hot halo around the laser-heated tracer. A generalized Stokes−Einstein relation for "hot Brownian motion" is developed and verified. Exploiting the excellent photostability of gold nanoparticles, the developed method promises broad applications especially in the field of quantitative biomedical screening.

Introduction

Fluorescence based methods with single molecule sensitivity have attracted large interest during the last years since they are capable of measuring local physical properties.[1−3] Especially fluctuation-based techniques such as fluorescence correlation spectroscopy (FCS)[4−6] have found rich applications in biophysics to study biochemical reactions[4,7,8] and molecular dynamics[9−11] even in living cells[12] and are meanwhile used commercially in the high throughput screening analysis of proteins and cells.[13−15] All of these techniques analyze the temporal changes of a fluorescence signal arising from the emission of fluorescent probe molecules[6] or semiconductor nanoparticles.[16] Metal nanoparticles, which interact strongly with light due to collective excitations of the conduction electrons (plasmons), can in principle be used as a substitute for fluorescent markers. A great advantage would be that metal nanoparticles do not suffer from photoblinking or photophysical degradation. Particularly gold nanoparticles are physiologically inert and profit from a highly developed chemistry for biocompatible functionalization. However, establishing metal nanoparticles as a competitive replacement for fluorescent markers requires a detection technique with comparable detection speed and sensitivity, which is still missing.

Here, we introduce such a technique called photothermal correlation spectroscopy (PhoCS). It is based on the photothermal heterodyne detection of gold nanoparticles as developed by Berciaud et al.,[17] which exploits the heat released from a light absorbing particle. The resulting temperature gradient in the surrounding solvent can be detected optically due to a change of the refractive index with temperature. We show that this technique can be turned into a spectroscopic method by applying a correlation analysis qualitatively equivalent to that of FCS. As a demonstration, we study gold nanoparticle diffusion in water with a time resolution of 20 μs (comparable to typical FCS measurements) and particle radii as small as $R = 2.5$ nm.

Experimental Section

Gold nanoparticles with radii from $R = 2.5$ nm up to $R = 30$ nm were obtained from British Biocell International (BBI). The solutions were confined between two glass slides or kept in a glass capillary (inner diameter of 200 μm) during the studies. The experimental setup is based on a home-built confocal microscope using two collinear laser sources. A DPSS laser with $\lambda_{heat} = 532$ nm is used to heat the gold nanoparticles. Its intensity is modulated sinusoidally at a frequency $\Omega = 300$ kHz with an acousto-optic modulator (Isomet 1206C), corresponding to a theoretical time resolution 3.3 μs (Ω^{-1}). The second light source (Coherent Cube635) at $\lambda_{probe} = 635$ nm probes the local refractive index changes. Both beams are focused into the sample by the same objective lens (Olympus 100x/1.4NA), collected above the sample by a second objective (Olympus 60x/0.7NA) and imaged on a photodiode (Thorlabs PDA36A). The light of the transmitted heating beam is blocked by appropriate filters (Omega Optical). The photodiode signal is analyzed by a lock-in amplifier (Signal Recovery, SR7280) with time constant set to $\tau_{LI} = 20$ μs. The demodulated signal of the lock-in amplifier is recorded in two channels (X and Y) by an A/D converter (ADWIN gold) every 20 μs (each trace lasting about 300 s). The digitized time traces are used to calculate the photothermal signal amplitude $\Phi = \sqrt{X^2 + Y^2}$. The noise level, which is largely electronic in origin, has been subtracted from all time traces before calculating the photothermal autocorrelation function.

Theoretical

According to the theory of photothermal heterodyne detection by Berciaud et al.,[18] the time-dependent local temperature increment around a nanoparticle periodically heated at frequency Ω is very well described by

* To whom correspondence should be addressed. E-mail: raduenz@physik.uni-leipzig.de.
† Institute of Experimental Physics I.
‡ Institute of Theoretical Physics.

10.1021/jp810466y CCC: $40.75

$$T(r,t) - T_a = \Delta T R/r[1 + e^{-r/R_{th}} \cos(\Omega t - r/R_{th})] \quad (1)$$

Here, $\Delta T = P_{abs}/(4\pi KR)$ is the surface temperature increment relative to the ambient temperature T_a, K and R_{th} are the thermal conductivity of the medium and the thermal skin depth, and r is the distance from the particle center and time t. Since the particle diffusion through the focus is slow compared to Ω^{-1}, the time-averaged eq 1, $T(r,t) - T_a = \Delta TR/r$, suffices for the following. We assume an absorbed heating laser power $P_{abs} = \sigma_{abs} I_{heat}$ (absorption cross section times incident intensity). The local temperature rise results in a local refractive index change $\Delta n(r,t) = [T(r,t) - T_a]\partial n/\partial T$ that scatters the probe laser beam. The resulting photothermal signal $\Phi \propto I_{heat} I_{probe} \sigma_{abs}$ is directly proportional to the heating laser intensity, the absorption cross section σ_{abs}, and the probe laser intensity.[18] The intensities I_{heat} and I_{probe} depend on the position of the particle inside the focus, and also σ_{abs} can in general be time dependent. The photothermal signal Φ will thus be sensitive to fluctuations of various origins, corresponding to a variety of possible microscopic observables. They are quantified by the autocorrelation function

$$G(\tau) = \langle \Phi(t)\Phi(t+\tau)\rangle / \langle \Phi(t)\rangle^2 \quad (2)$$

to extract the characteristic time scale τ_D of the underlying processes, which is understood to be well separated from the modulation time scale Ω^{-1} used in the lock-in detection.

In the remainder, we exemplarily focus on the study of tracer diffusion as the source of photothermal signal fluctuations. The basic principle of diffusion studies by photothermal correlation spectroscopy is equivalent to FCS. We can therefore closely follow the FCS data analysis procedure and apply it to the photothermal signal. For Gaussian shaped heating and probe beam intensity distributions with different lateral extensions ω_ρ^{heat} and ω_ρ^{probe} and axial extensions ω_z^{heat} and ω_z^{probe}, but the same focal position, the detected signal obeys

$$\Phi \propto \exp\left[-\frac{2\rho^2}{(\omega_\rho^{heat})^2} - \frac{2z^2}{(\omega_z^{heat})^2}\right] \exp\left[-\frac{2\rho^2}{(\omega_\rho^{probe})^2} - \frac{2z^2}{(\omega_z^{probe})^2}\right] \quad (3)$$

resulting in a Gaussian detection probability distribution (even in the case where both beams are displaced in the focal plane or along the optical axis). Thus the photothermal detection volume can be described by its two semiaxes ω_ρ, ω_z

$$\omega_{\rho,z} = \omega_{\rho,z}^{heat} \omega_{\rho,z}^{probe} [(\omega_{\rho,z}^{heat})^2 + (\omega_{\rho,z}^{probe})^2]^{-1/2} \quad (4)$$

corresponding to the effective focal volume extension in the lateral and axial directions. The photothermal signal is in the same way directly proportional to the number of gold nanoparticles in the focal volume[19] as the fluorescence signal in FCS, which relates the intensity fluctuations in both techniques to concentration fluctuations in the focal volume. Due to this equivalence, we can adopt the FCS autocorrelation function for photothermal correlation spectroscopy

$$G(\tau) = 1 + \langle N\rangle^{-1}(1 + \tau/\tau_D)^{-1}(1 + \gamma^2\tau/\tau_D)^{-1/2} \quad (5)$$

with $\langle N\rangle$ being the average number of particles in the focal region, $\tau_D = \omega_\rho^2/4D$ as the characteristic diffusion time, and $\gamma = \omega_\rho/\omega_z$ a factor describing the ratio of the lateral and axial extension of the effective focal region formed by both lasers (see Figure 1).

Compared to FCS, the tracer induces, however, a temperature gradient in its vicinity, which is the basis of photothermal detection. The heating causes a local viscosity gradient and an increase in the strength of thermal fluctuations around the particle, which modifies its Brownian motion. Also the focus geometry changes in response to the heat induced refractive index change. Thus a principal prerequisite for applying the technique is to control these heating effects and to quantify their importance. Since heat diffuses much faster than the tracer, both temperature and viscosity vary radially around its center. Accordingly, the strength of the thermal forces that drive Brownian motion decays and the friction that impedes it typically rises with increasing distance from the particle. Yet, as we demonstrate below, a generalized Stokes−Einstein relation

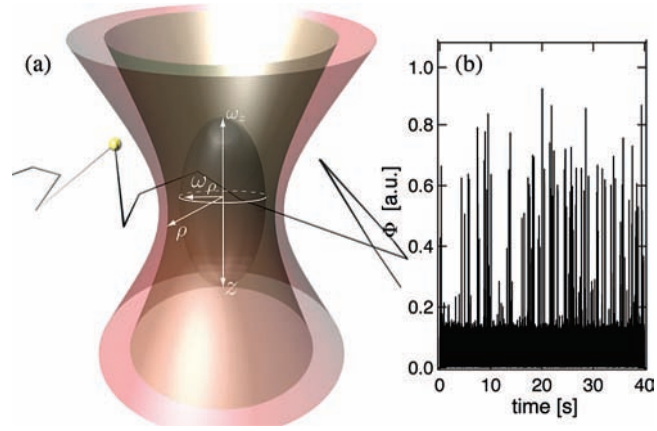

Figure 1. PhoCS detection scheme (a) with overlapping foci of the heating (green) and the detection (red) laser. The ellipsoid represents the focal volume with two principal axes ω_z and ω_ρ. Exemplary photothermal signal timetrace (b) for gold nanoparticles with $R = 20$ nm in water, heating power 0.5 mW, probe beam power 1 mW.

$$\tau_D = \omega_\rho^2/(4\tilde{D}) = 6\pi\tilde{\eta}R\omega_\rho^2/(4k_B\tilde{T}) \quad (6)$$

still holds for an appropriately defined effective temperature $\tilde{T}$, viscosity $\tilde{\eta}$, and diffusion coefficient $\tilde{D}$. To theoretically estimate $\tilde{\eta}$ one needs to calculate the divergence-free velocity field $\boldsymbol{u}$ from the stationary Stokes equation

$$0 = -\nabla p + \nabla \cdot (\eta \nabla \boldsymbol{u}) \quad (7)$$

for an incompressible fluid of constant density and radially varying viscosity $\eta(r)$, with pressure p, which simply expresses the conservation of the momentum flux. The force per unit area exerted by the fluid onto a moving sphere is given by the normal projection of the momentum flux onto the surface of the sphere, which upon integration over the sphere's surface yields the total force. For constant viscosity $\eta(r) = \eta_0$, explicit calculations[20] show that both contributions in eq 7 factorize into angular and radial parts, and moreover contribute equal amounts to the total force. Thus, it is tempting to consider in place of eq 7 the much simpler diffusion problem

$$0 = \nabla \cdot (\eta \nabla u) = (\nabla\eta) \cdot (\nabla u) + \eta\nabla^2 u \quad (8)$$

to which eq 7 degenerates for a fictitious scalar "velocity" u. However, even for a spatially constant viscosity, this procedure yields an incorrect numerical prefactor of 4π instead of 6π in Stokes' law $F = 6\pi\eta R$v, due to the wrong boundary condition on the surface of the sphere. On the other hand, if this known mismatch is corrected manually, one may indeed expect the effective friction for a radially varying viscosity, which can be calculated analytically from eq 8, to provide an accurate approximation to the exact result, which would have to be obtained numerically for each particular parameter set of interest from eq 7. In the following, we pursue this approximate analytical route,[21] which turns out to be in very reasonable accord with our experimental results.

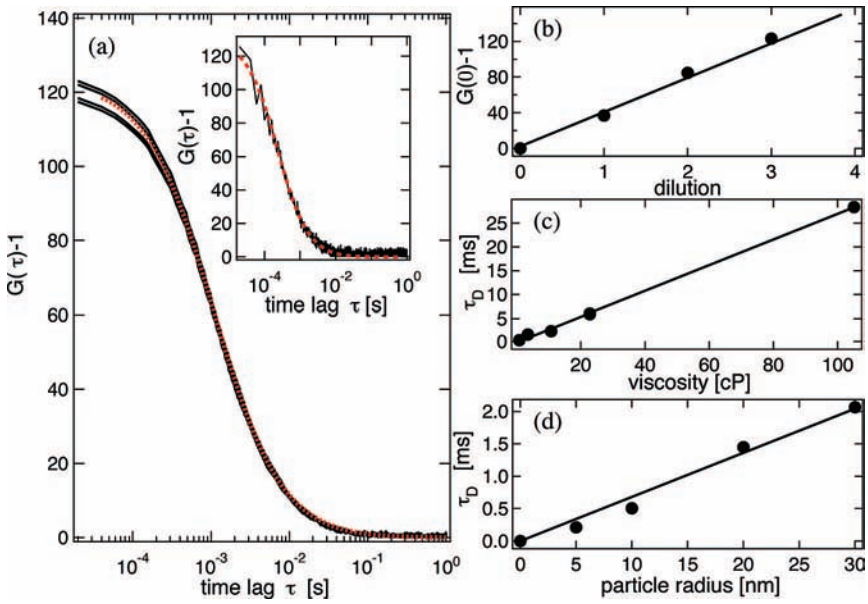

Figure 2. (a) Photothermal autocorrelation function for four different measurements (solid lines) of $R = 30$ nm particles in water together with a fit using eq 5 (dashed line). The inset shows the correlation function for the diffusion of $R = 2.5$ nm particles in water. (b) Contrast $G(\tau = 0) - 1$ of the photothermal autocorrelation function at different dilution (volume fraction) of the original gold nanoparticle solution. (c) Dependence of the diffusion time τ_D for $R = 30$ nm on the viscosity of a glycerol water mixture. The viscosity of the mixture has been calculated from the mass fraction.[24] (d) Dependence of the diffusion time τ_D as a function of the particle radius R.

To model the temperature dependence of the viscosity, we use the phenomenological expression

$$\log(\eta/\eta_0) = B/(T - T_K) \tag{9}$$

with parameters $\eta_0 = 2.984 \times 10^{-5}$ mPa s, $B = 496$ K, $T_K = 150$ K (Kauzmann temp.),[22] and the radial temperature dependence $T(r) = T_a + \Delta T R/r$ from above. The solution of eq 8 results in $u(r) = \text{const} \cdot v(r)$ with

(10) 0″ position=″anchor″>

$$v(r) = -\frac{2}{3}[(T_0/\Delta T + R/r)e^{-x} - B/\Delta T \mathrm{Ei}(-x)] \tag{10}$$

where $x \equiv rB/(rT_0 + R\Delta T)$ and $T_0 \equiv T_a - T_K$. Thus, we obtain the effective viscosity $\tilde{\eta}$

$$\tilde{\eta} = \eta_0/[\lim_{x\to\infty} v(r) - v(R)] \tag{11}$$

A detailed theoretical treatment of the spatially extended thermal fluctuations contributing to the effective temperature $\tilde{T}$ is less straightforward,[21] but a consistent estimate is provided by the temperature that corresponds to the effective viscosity $\tilde{\eta}$ via eq 9, i.e.,

$$\tilde{T} = B/\log(\tilde{\eta}/\eta_0) + T_K \tag{12}$$

Altogether, the particle diffusion time τ_D is calculated by inserting expressions (10), (11), and (12) into the generalized Stokes−Einstein relation (6).[23]

Several other influences of the heating, such as thermophoretic trapping, and the variation of the solvent density and index of refraction, and, correspondingly, of the focus geometry, have been theoretically estimated to be subdominant and were therefore dismissed in our analysis. A more detailed discussion of their contributions will be given in future work.

Results and Discussion

Figure 2 presents four autocorrelation functions as obtained from subsequent measurements together with a fit using eq 5. It demonstrates the high data quality (low noise) and low scatter between subsequent measurements. The autocorrelation function is well described by eq 5 with only minor deviations, thereby providing an experimental proof that eq 5 applies to PhoCS.

Also shown in Figure 2 are the linear dependencies on ambient viscosity and particle radius, which corroborate the generalized Stokes−Einstein relation, eq 6. Particle radii range from $R = 5$ up to 30 nm, and the size dependence of σ_{abs}[25] has been taken into account. The viscosity dependence was measured using $R = 30$ nm particles in a glycerol/water mixture at different glycerol content and constant heating power. Comparing the diffusion times at different heating power requires a more detailed knowledge of the hydrodynamics of a particle in a local viscosity and temperature gradient. To quantify this influence experimentally, we have determined $G(\tau)$ for $R = 20$ and 30 nm gold nanoparticles in water at various heating powers. Figure 3 depicts the measured diffusion times as a function of the incident heating power and of the surface temperature increment ΔT. The figure clearly reveals the anticipated speed-up of diffusion with heating.

Using both the effective viscosity $\tilde{\eta}$ and the effective temperature $\tilde{T}$ (as outlined above) to calculate the diffusion time τ_D, we obtain the results shown in the inset of Figure 3 as solid lines. There is good agreement with the temperature dependence observed in the experiment. Note that the experimental diffusion times have been rescaled by the constant factors 1.7 and 1.4 for the $R = 20$ and 30 nm particles, respectively, in order to bring the data closer to the theoretical predictions, which involve no free parameters. This is justified by the fact that the absolute value of the experimentally measured diffusion time is, as in the case of FCS, only known with low precision due to various poorly controlled influences, such as the cover slide thickness or precise focus geometry.[26] The problem could be overcome in a double focus version[27] of the described setup, which is currently under development.

Conclusions

The experimental and theoretical results presented above clearly demonstrate that "hot Brownian motion" is an interesting

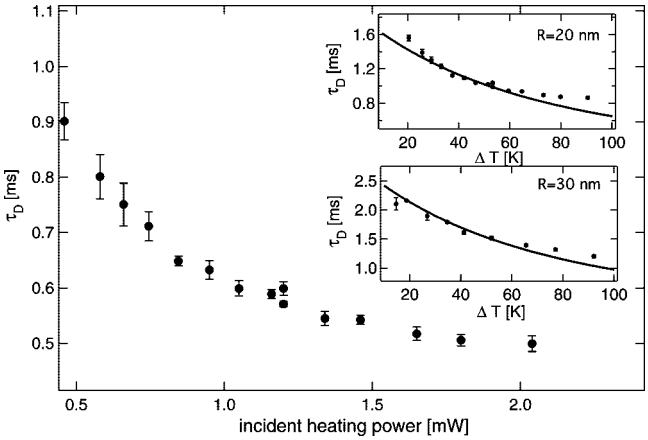

Figure 3. Experimentally determined diffusion time τ_D of $R = 20$ nm particles in water at different incident heating powers. The insets show the diffusion times over the nanoparticle surface temperature estimated from eq 1 assuming absorption cross sections of 2199 nm^2 for $R = 20$ nm and 7424 nm^2 for $R = 30$ nm particles,[25] and a focus size of $\omega_\rho = 300$ nm. The solid lines represent the theoretical predictions of eq 11 with scaling factors 1.4 and 1.7 for the $R = 30$ and 20 nm measurement, respectively.

nonequilibrium transport phenomenon that can advantageously be exploited in a new measurement technique, PhoCS. PhoCS is able to deliver the same general results on diffusion as FCS does. Fluorescent tracers as used in FCS can thus be replaced by photostable nonfluorescent tracers of almost equivalent size, keeping the general formalism as familiar from FCS. Further, the integration of a photothermal microscopy setup in a confocal microscopy scheme with an equivalent optical resolution allows the use of common FCS setups. In contrast to FCS no expensive single photon counting hardware is required to achieve single particle sensitivity. While scattering detection of small particles $R < 20$ nm is difficult, especially in heterogeneous environments, photothermal heterodyne detection has been successful in detecting gold particles as small as $R = 0.7$ nm as well as nanoparticles in living cells.[17,19] Due to the fact that PhoCS relies on the absorption of a species in a nonabsorbing environment and employs a lock-in based detection it is background-free and highly selective.[17,25] As the photothermal signal fluctuations can be caused not only by particle diffusion through a focal volume but also by distance dependent coupling of plasmon resonances of nearby nanoparticles[28,29] or local dielectric changes,[30,31] which can be exploited in a broad range of applications, PhoCS promises to become a versatile tool for the study of a large variety of dynamical processes on the nanoscale.

Acknowledgment. This work profited from fruitful discussions with and technical support by Achim Gruber, Rüdiger Kürsten, and Helge K. Nete and was funded by the Deutsche Forschungsgemeinschaft via FOR 877 and, within the German excellence initiative, the Leipzig School of Natural Sciences "Building with molecules and nano-objects".

Supporting Information Available: The complete formula joining the theoretical results of the effective viscosity calculation and the effective temperature formula. This material is available free of charge via the Internet at http://pubs.acs.org.

References and Notes

(1) Moerner, W. E.; Orrit, M. *Science* **1999**, *283*, 1670–1676.
(2) Zondervan, R.; Kulzer, F.; Berkhout, G. C.; Orrit, M. *Proc. Natl. Acad. Sci. U.S.A.* **2007**, *104*, 12628–12633.
(3) Barth, M.; Schuster, R.; Gruber, A.; Cichos, F. *Phys. Rev. Lett.* **2006**, *96*, 243902.
(4) Magde, D.; Elson, E.; Webb, W. W. *Phys. Rev. Lett.* **1972**, *29*, 705–708.
(5) Schwille, P.; Korlach, J.; Webb, W. W. *Cytometry* **1999**, *36*, 176–182.
(6) Krichevsky, O.; Bonnet, G. *Rep. Prog. Phys.* **2002**, *65*, 251–297.
(7) Nishimura, G.; Kinjo, M. *Biophysics* **1999**, *39*, 81–85.
(8) Henzler-Wildman, K. A.; Thai, V.; Lei, M.; Ott, M.; Wolf-Watz, M.; Fenn, T.; Pozharski, E.; Wilson, M. A.; Petsko, G. A.; Karplus, M.; Hubner, C. G.; Kern, D. *Nature* **2007**, *450*, 838–844.
(9) Bonnet, G.; Krichevsky, O.; Libchaber, A. *Proc. Natl. Acad. Sci. U.S.A.* **1998**, *95*, 8602–8606.
(10) Korlach, J.; Schwille, P.; Webb, W. W.; Feigenson, G. W. *Proc. Natl. Acad. Sci. U.S.A.* **1999**, *96*, 8461–8466.
(11) Petrov, E. P.; Ohrt, T.; Winkler, R. G.; Schwille, P. *Phys. Rev. Lett.* **2006**, *97*, 258101.
(12) Kim, S. A.; Heinze, K. G.; Schwille, P. *Nat. Methods* **2007**, *4*, 963–973.
(13) Eigen, M.; Rigler, R. *Proc. Natl. Acad. Sci. U.S.A.* **1994**, *91*, 5740–5747.
(14) Auer, M.; Moore, K. J.; Meyer-Almes, F. J.; Guenther, R.; Pope, A. J.; Stoeckli, K. A. *Drug Discovery Today* **1998**, *3*, 457–465.
(15) Sundberg, S. A. *Curr. Opin. Biotechnol.* **2000**, *11*, 47–53.
(16) Larson, D. R.; Zipfel, W. R.; Williams, R. M.; Clark, S. W.; Bruchez, M. P.; Wise, F. W.; Webb, W. W. *Science* **2003**, *300*, 1434–1436.
(17) Berciaud, S.; Cognet, L.; Blab, G. A.; Lounis, B. *Phys. Rev. Lett.* **2004**, *93*, 257402.
(18) Berciaud, S.; Lasne, D.; Blab, G. A.; Cognet, L.; Lounis, B. *Phys. Rev. B* **2006**, *73*, 045424.
(19) Cognet, L.; Tardin, C.; Boyer, D.; Choquet, D.; Tamarat, P.; Lounis, B. *Proc. Natl. Acad. Sci. U.S.A.* **2003**, *100*, 11350–11355.
(20) Lifshitz, E. M.; Pitaevskii, L. P. *Fluid Mechanics*; Elsevier: Amsterdam, 2004.
(21) Rings, D. ; Radünz, R.; Cichos, F.; Kroy, K. in preparation.
(22) Eisenberg, D.; Kauzmann, W. *The Structure and Properties of Water*; Oxford University Press: Oxford, 2005.
(23) This information is available free of charge via the Internet at http://pubs.acs.org.
(24) Chen, Y.-M.; Pearlstein, A. J. *Ind. Eng. Chem. Res.* **1987**, *26*, 1670–1672.
(25) van Dijk, M. A.; Tchebotareva, A. L.; Orrit, M.; Lippitz, M.; Berciaud, S.; Lasne, D.; Cognet, L.; Lounis, B. *Phys. Chem. Chem. Phys.* **2006**, *8*, 3486–3495.
(26) Enderlein, J.; Gregor, I.; Patra, D.; Fitter, J. *Curr. Pharm. Biotechnol.* **2004**, *5*, 155–161.
(27) Dertinger, T.; Loman, A.; Ewers, B.; Müller, C. B.; Krämer, B.; Enderlein, J. *Opt. Expr.* **2008**, *16*, 14353.
(28) Sönnichsen, C.; Reinhard, B. M.; Liphardt, J.; Alivisatos, A. P. *Nat. Biotechnol.* **2005**, *23*, 741–745.
(29) Stehr, J.; Hrelescu, C.; Sperling, R. A.; Raschke, G.; Wunderlich, M.; Nichtl, A.; Heindl, D.; Kurzinger, K.; Parak, W. J.; Klar, T. A.; Feldmann, J. *Nano Lett.* **2008**, *8*, 619–623.
(30) Kreibig, U.; Vollmer, M. *Optical properties of Metal Clusters*; Springer: Heidelberg, 1995.
(31) Miller, M. M.; Lazarides, A. A. *J. Opt. A* **2006**, *8*, S239−S249.

JP810466Y